FORMATIONS NEAR THE LIBRATION POINTS:
DESIGN STRATEGIES USING NATURAL AND NON-NATURAL ARCS

K.C. HOWELL and B.G. MARCHAND

Space based observatory and interferometry missions, such as Terrestrial Planet Finder (TPF), Stellar Imager, and MAXIM, have sparked great interest in multi-spacecraft formation flight in the vicinity of the Sun-Earth/Moon (SEM) libration points. The initial phase of this research considered the formation keeping problem from the perspective of continuous control as applied to non-natural formations. In the present study, closer inspection of the flow, corresponding to the stable and center manifolds near the reference orbit, reveals some interesting natural relative motions as well as some discrete control strategies for deployment. A hybrid control strategy is also employed that combines both the natural formation dynamics with non-natural motions via input feedback linearization techniques.

INTRODUCTION

Much of the available research on formation flight focuses on Earth orbiting configurations [1-16], where the influence of other gravitational perturbations can be safely ignored. However, renewed interest in formations that evolve near the vicinity of the Sun-Earth libration points has inspired new studies regarding formation keeping in the three-body problem [17-32]. Some of these investigations focus on the simplified circular restricted three-body problem (CR3BP) [17-20, 30]. Previous studies [30] consider linear optimal control, as applied to nonlinear time varying systems, as well as nonlinear control techniques, including input and output feedback linearization. That analysis is initially performed in the CR3BP, but is later transitioned into the more complete ephemeris (EPHEM) model [31-32]. These control strategies are applied to a two spacecraft formation where the chief spacecraft (i.e., the central vehicle in the formation) evolves along a three-dimensional periodic halo orbit near the L_1 and L_2 libration points. The deputy vehicle, through continuous thrusting, is then commanded to follow a non-natural arc relative to the chief.

This particular effort does not constitute the only application of continuous control techniques in the CR3BP. Scheeres and Vinh [17] develop a non-traditional yet innovative continuous controller, based on the local eigenstructure of the linear system, to achieve bounded motion near the vicinity of a halo orbit. Other research efforts have also focused on the effectiveness of continuous control techniques in the general CR3BP, though not in the vicinity of the libration points. Gurfil and Kasdin, for instance, consider both LQR techniques [18] and adaptive neural control [19] for formation keeping in the CR3BP. The second approach, described in [19], incorporates uncertainties introduced by modeling errors, inaccurate measurements, and external disturbances. Luquette and Sanner [20] apply adaptive nonlinear control to address the same sources of uncertainties in the nonlinear CR3BP.

Formations modeled in the CR3BP do represent a good starting point. However, ultimately, any definitive formation keeping studies must be performed in the *n*-body ephemeris (EPHEM) model, where the time invariance properties of the CR3BP are lost and, consequently, precisely periodic orbits do not exist near the libration points. Hamilton [21] and Folta et al. [22] consider linear optimal control for formation flight relative to Lissajous trajectories, as determined in the EPHEM model. In their study, the evolution of the controlled formation is approximated from a linear dynamical model relative to the integrated reference orbit. Finally, Howell and Barden [23-26] also investigate formation flying near the vicinity of the libration points in the perturbed Sun-Earth/Moon system. Their results are determined in the full nonlinear EPHEM model.

Initially, their focus is the determination of the natural behavior on the center manifold near the libration points and the first step of their study captures a naturally occurring six-satellite formation near L_1 or L_2 [23]. Further analysis considers strategies to maintain a planar formation of the six vehicles in an orbit about the Sun-Earth L_1 point [24-26], that is, controlling the deviations of each spacecraft relative to the initial formation plane.

A discrete station keeping/control approach is devised to force the orientation of the formation plane to remain fixed inertially. An alternate approach is also implemented by Gómez et al. [27] in a study of the deployment and station keeping requirements for the TPF nominal configuration. Their analysis is initially performed in a simpler model but the simulation results are transitioned into the EPHEM model.

In the present study, two types of impulsive control are presented as well as a hybrid continuous control method that exploits the natural formation dynamics near the libration points. Among the impulsive schemes considered, a targeter approach that is, in concept, similar to that implemented by Howell and Barden [24-26] in the EPHEM model is incorporated. This particular controller is applied here to formation configurations defined in the inertial frame. In addition, the station keeping techniques previously implemented by Howell and Keeter [28] and Gómez et al. [29], based on a Floquet controller, are adapted to the formation keeping problem. In particular, the Floquet controller is applied to study naturally existing formations near the libration points and the potential deployment into such configurations. These natural relative motions are later combined with a continuous input feedback linearization approach to construct hybrid non-natural reference motions. Hybrid solutions allow for significant thruster down times over certain trajectory arcs. However, continuous control is still required over some segments of the path.

DYNAMICAL MODEL

Circular Restricted Three-Body Model

There are a variety of ways to formulate the dynamical model of a spacecraft (S/C) formation. In this study, the central spacecraft is termed "chief" while all other vehicles in the formation are denoted as "deputies". In the CR3BP, the motion of the chief S/C is described in terms of rotating coordinates (R) relative to the barycenter (B) of the system primaries (SEM system). In this frame, the rotating x-axis is directed from the Sun towards the Earth-Moon barycenter, as illustrated in Figure 1.
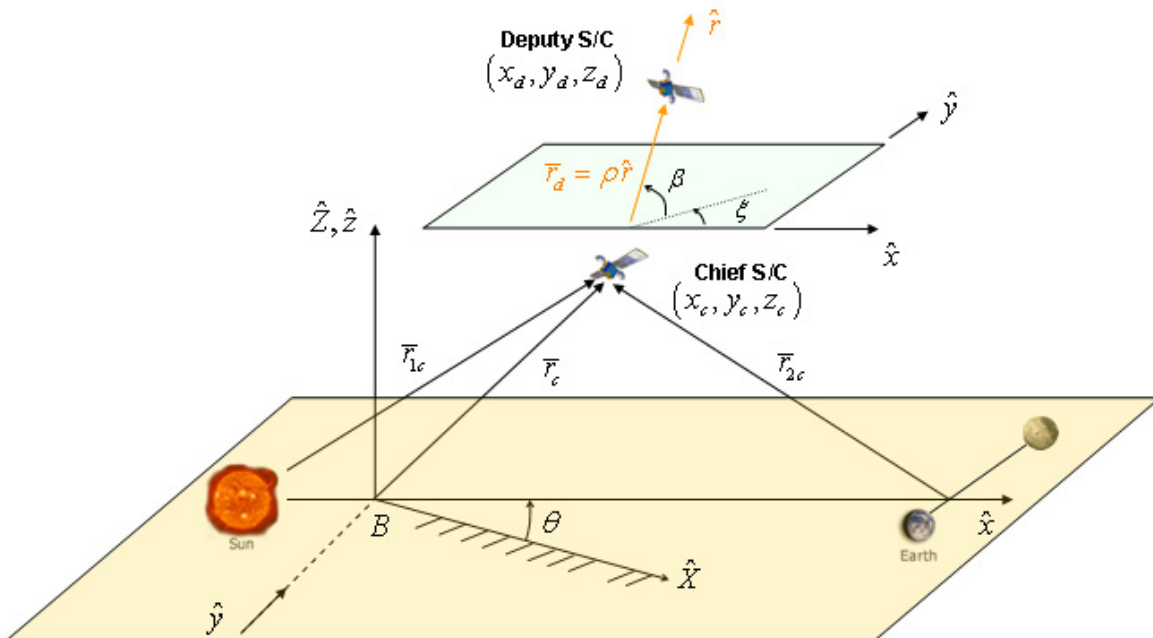

Figure 1 - Two S/C Formation Model in the Sun-Earth-Moon CR3BP

The z-axis is normal to the plane of motion of the primaries, and the y-axis completes the right-handed triad. Alternatively, in the ephemeris model, the frame of reference is inertial (I) and Earth centered (P_2). In either formulation, equations of motion for either the chief or the deputy vehicle, relative to a reference point Q (B or P_2), can be expressed, in a general form, as

$$\ddot{\overline{r}}(t) = \overline{f}\left(\overline{r}_d(t), \dot{\overline{r}}_d(t)\right) - \overline{f}\left(\overline{r}_c(t), \dot{\overline{r}}_c(t)\right) + \overline{u}_d(t) - \overline{u}_c(t) = \Delta\overline{f}\left(\overline{r}(t), \dot{\overline{r}}(t)\right) + \Delta\overline{u}(t). \tag{1.1}$$

The subscript "c" indicates that the function is associated with the chief spacecraft while the subscript "d" implies evaluation along the path of the deputy. The position vectors $\overline{r}_c$ and $\overline{r}_d$, then, locate the chief and deputy vehicles relative to the reference point Q, respectively. The vector $\overline{r} = \overline{r}_d - \overline{r}_c = [x, y, z]^T$ locates the deputy spacecraft relative to the chief vehicle. The quantity $\Delta\overline{f} = \left[\Delta f_x, \Delta f_y, \Delta f_z\right]^T$ represents the vector sum of the net forcing terms acting on the vehicles as well as any kinematic terms that <u>may</u> be present due to the working frame associated with the specified formulation. In the present investigation, the chief spacecraft is assumed to evolve along a naturally existing solution such that $\overline{u}_c(t) = 0$, hence $\Delta\overline{u}(t) = \overline{u}_d(t)$.

Ephemeris Dynamical Model

The ephemeris model is based on the standard relative equations of motion for the n-body problem, as formulated in the inertial frame (I). The equations are, however, modified to include the effects of solar radiation pressure (SRP). Hence, the dynamical evolution of each vehicle in the formation, relative to the Earth, is governed by

$$^I\ddot{\overline{r}}^{P_2 P_s} = -\frac{\mu_{P_2}}{\left(r^{P_2 P_s}\right)^3} + \sum_{j=1, j\neq 2, s}^{N} \mu_{P_j}\left(\frac{\overline{r}^{P_s P_j}}{\left(r^{P_s P_j}\right)^3} - \frac{\overline{r}^{P_2 P_j}}{\left(r^{P_2 P_j}\right)^3}\right) + \overline{f}_{srp}^{(P_s)}. \tag{1.2}$$

For notational purposes, let P_2 denote the central body of integration, in this case the Earth. Then, P_s represents the spacecraft, and the sum over j symbolizes the presence of other gravitational perturbations. Note that μ_{P_2} and μ_{P_j} represent the gravitational parameters of the central body, P_2, and the jth perturbing body, P_j, respectively. The SRP force vector, as discussed by McInnes [33], is modeled as

$$\overline{f}_{srp}^{(P_s)} = \frac{k S_0 A}{m_s c}\left(\frac{D_0^2}{d^2}\right)\cos^2\beta \; \hat{n}, \tag{1.3}$$

where k denotes the absorptivity of the spacecraft surface ($k = 2$ for a perfectly reflective surface), S_0 is the energy flux measured at the Earth's distance from the Sun [W·m^{-2}], D_0 is the mean Sun-Earth distance [km], A represents the constant spacecraft <u>effective</u> cross sectional area [km^2], c is the speed of light [km·s^{-1}], m_s is the spacecraft mass [kg], β is the angle of incidence of the incoming photons, $\hat{n}$ denotes the unit surface normal, and d [km] represents the Sun-spacecraft distance.

DISCRETE FORMATION KEEPING

Based on results from previous investigations, [18-20, 30-32] it appears that it is possible, at least computationally, to achieve precise formations in the CR3BP and in the EPHEM model, that is, <u>if</u> continuous control is both available and feasible. Past studies [30-32] demonstrate that, depending on the constraints imposed on the formation configuration, a continuous control approach may nominally require thrust levels ranging from 10^{-3} to 10^{-9} Newtons. In contrast, the present state of propulsion technology allows for operational thrust levels on the order of 90-1000 μN via pulsed plasma thrusters, such as those available for attitude control onboard EO-1 [34]. Of course, increased interest in micro- and nano-satellites continues to motivate theoretical and experimental studies to further lower these thrust levels, as discussed by Mueller [35], Gonzalez [36], and Phipps [37]. Gonzalez [36] estimates that a lower bound of 0.3 nN is possible via laser induced ablation of aluminum. Aside from their immediate application to micro- and nano-satellite missions, these concepts are also potentially promising for formation flight near the libration points.

Ultimately, the level of accuracy achievable in tracking the nominal motion, for a given configuration, depends strongly on the ability to deliver the required thrust levels accurately. Although continuous control approaches are mathematically sound, the science goals of deep space missions may impose a series of constraints that eliminate continuous control as a feasible option. Some also suggest that maintaining a precise formation is, perhaps, ultimately not as critical as generating precise knowledge of the relative position of each spacecraft in the formation. In these cases, a discrete formation keeping strategy may represent an important capability.

Investigation of various discrete control strategies

In this study, two discrete control strategies are considered for formation keeping. Both of these rely on knowledge of the linearized dynamics associated with the reference orbit, but incorporate the nonlinear response of the vehicle. In this case, the reference orbit is the path of the chief spacecraft, assumed to evolve along a 2×10^5 km halo orbit, as determined in the Sun-Earth/Moon ephemeris (EPHEM) system. The deputy dynamics, then, are modeled as a perturbation relative to the reference orbit. The success of a particular control strategy depends, in part, on the nominal motion that is required of the deputy.

In the first method, a linear targeter is applied to enforce a non-natural formation. The control goal is to enforce either (a) some pre-specified relative deputy state, or (b) a nominal radial distance and rate. Since this type of motion does not exist naturally near the libration points, continuous control is necessary to <u>precisely</u> enforce the formation for the duration of the mission. This "precise" control assumes that the goals of the mission require formation keeping accuracies below 10^{-3} m. Here, instead of applying continuous control, the path of the deputy is divided into segments. At the beginning of each segment, an impulsive maneuver is implemented that targets a specific end state constraint. If the nominal separation between the chief and deputy spacecraft is small, this approach proves to be effective if the required tolerances are on the order of 10^{-2} m. Whether this represents an acceptable tolerance level depends on the goals of the mission. For instance, as presently envisioned, missions like Stellar Imager require that the nominal vehicle configuration be maintained to within 10^{-6} m. The results from earlier studies [30-32] clearly indicate, then, the need for continuous formation control if non-natural relative motions are of interest.

Alternatively, a controller derived from Floquet analysis [31], based on the reference orbit, is employed here to remove the unstable component of the relative state, as well as two of the four center subspace modes that are associated with the reference orbit. The path of the deputy, then, is representative of a synthesis between the stable and center flows. In contrast with the first method, this type of control does <u>not</u> target a non-natural reference motion. Instead, the control scheme nominally places the deputy spacecraft on a naturally existing path that exhibits nearly periodic behavior, bounded motion, or quasi-periodic motion relative to the chief spacecraft. The control essentially seeks to return the deputy to this natural path.

DISCRETE CONTROL OF NON-NATURAL FORMATIONS IN THE EPHEMERIS MODEL

Driven by control and/or implementation requirements, some new consideration is warranted concerning the degree of accuracy to which the formation can be maintained via discrete impulses. Among the available alternatives, a discrete Linear Quadratic Regulator (LQR) yields the optimal magnitude of each differential control impulse at specified time intervals. This approach is well suited for station keeping of natural solutions, such as Lissajous trajectories or halo orbits, which nominally require no control. However, non-natural solutions do require a nominal control input. The value of the nominal control input that must be added is still assumed to be continuously available. Hence, the LQR method, in this case, does not yield a truly discrete formation keeping strategy. The present analysis considers other impulsive control alternatives as well as the implications associated with a non-continuous control approach.

Targeting a nominal relative state

Consider a formation where the chief spacecraft evolves along the Lissajous trajectory plotted in Figure 2, near the SEM L_2 point. Note that this trajectory is determined in the EPHEM model. Furthermore, let the nominal state of the deputy be defined by the position vector $\bar{\rho}(t)$, measured from the chief to the deputy, and the relative velocity vector $\dot{\bar{\rho}}(t)$. In the present example, $\bar{\rho}(t) = (100 \text{ km})\hat{Y}$ and $\dot{\bar{\rho}}(t) = \bar{0}$.
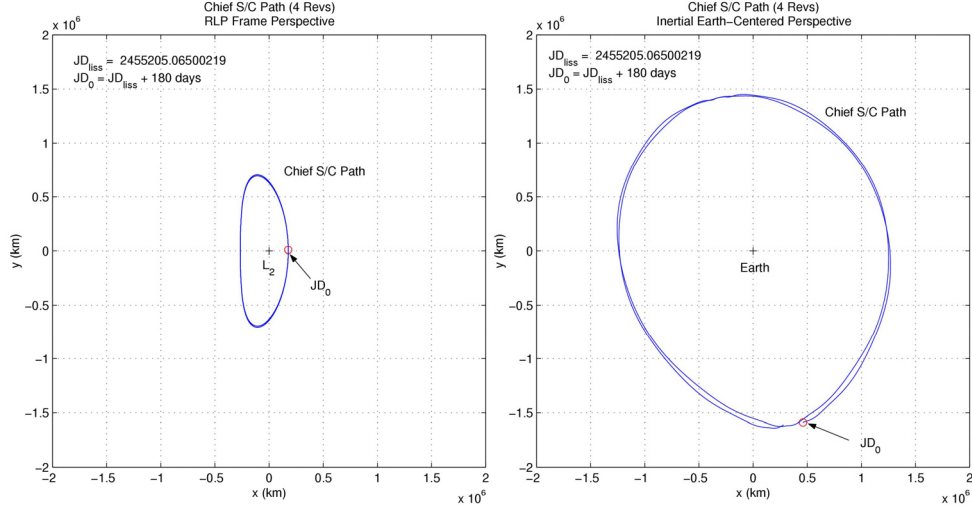
Figure 2 – Reference Lissajous trajectory for chief s/c path
(rotating and inertial frame perspectives).

Since this type of <u>relative</u> spacecraft motion is not consistent with the natural dynamics near the libration points, at least nearly continuous control is necessary for precise formation keeping. However, if the mission specifications allow some flexibility in the relative vehicle position tolerances, an impulsive control approach may be sufficient. The impulsive scheme presented here is based on a differential corrections approach derived from analysis of the linearized system dynamics.

The general solution to the equations representing the linear system may be written as,

$$\begin{bmatrix} \delta\bar{r}_{k+1} \\ \delta\dot{\bar{r}}_{k+1}^{-} \end{bmatrix} = \Phi(t_{k+1}, t_k) \begin{bmatrix} \delta\bar{r}_k \\ \delta\dot{\bar{r}}_k^{+} \end{bmatrix} = \begin{bmatrix} A_k & B_k \\ C_k & D_k \end{bmatrix} \begin{bmatrix} \delta\bar{r}_k \\ \delta\dot{\bar{r}}_k^{-} + \Delta\bar{V}_k \end{bmatrix}, \tag{1.4}$$

where $\Phi(t_{k+1}, t_k)$ denotes the state transition matrix, from time t_k to time t_{k+1}, associated with the <u>actual</u> deputy spacecraft path. The symbol δ denotes a perturbation relative to the actual deputy path and $\Delta\bar{V}_k$ represents an impulsive maneuver applied at the beginning of the kth segment, marked by t_k. In this case, $\delta\bar{r}_k = \bar{r}_k^{\circ} - \bar{r}_k$, $\delta\dot{\bar{r}}_k^{-} = \dot{\bar{r}}_k^{\circ} - \dot{\bar{r}}_k^{-}$, and $\delta\bar{r}_{k+1} = \bar{r}_{k+1}^{\circ} - \bar{r}_{k+1}$ where the superscript '$\circ$' denotes evaluation along the nominal deputy path. Thus, $\bar{r}_k^{\circ} = \bar{r}^{P_2C}(t_k) + \bar{\rho}^{\circ}(t_k)$ and $\dot{\bar{r}}_k^{\circ} = \dot{\bar{r}}^{P_2C}(t_k) + \dot{\bar{\rho}}(t_k)$, where '$P_2C$' denotes the distance from P_2 to the chief spacecraft. Controlling the position of the deputy spacecraft relative to the chief to a constant vector, as observed in the inertial frame, is equivalent to targeting a particular constant perturbation in position, $\delta\bar{r}_{k+1}$, relative to the inertial frame. An impulsive maneuver of the form

$$\Delta\bar{V}_k = B_k^{-1}\left(\delta\bar{r}_{k+1} - A_k\delta\bar{r}_k\right) - \delta\dot{\bar{r}}_k^{-}, \tag{1.5}$$

will accomplish the goal in the linear system. In the nonlinear EPHEM model employed here, a precise implementation of this scheme is accomplished through a differential corrections process performed over each segment, as discussed by Howell and Barden [24-26]. A sample implementation of this approach, in the EPHEM model, is presented in Figure 3. The maneuver strategies associated with each curve in Figure 3 are illustrated in Figure 4.
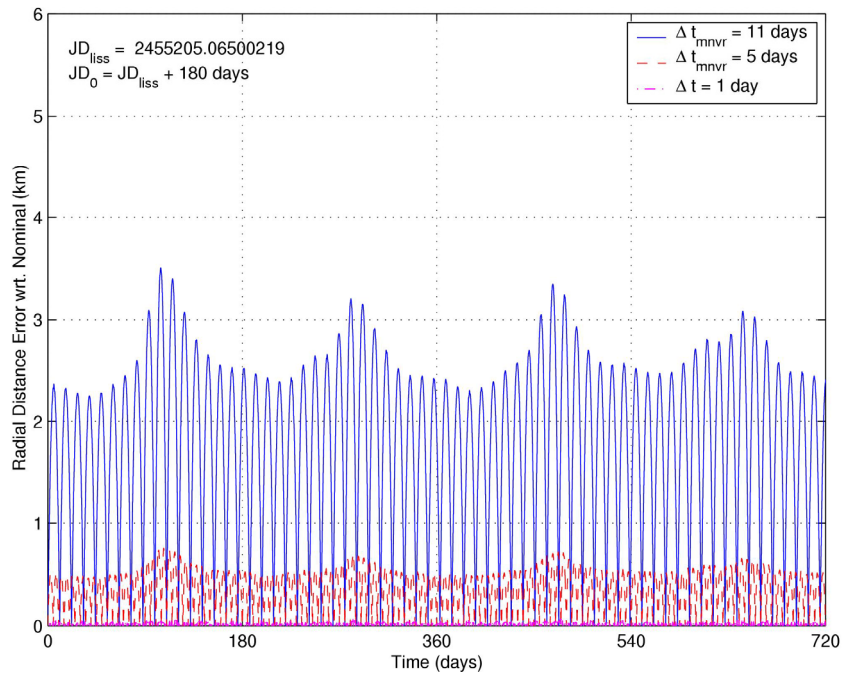
**Figure 3 – Position error relative to the nominal path
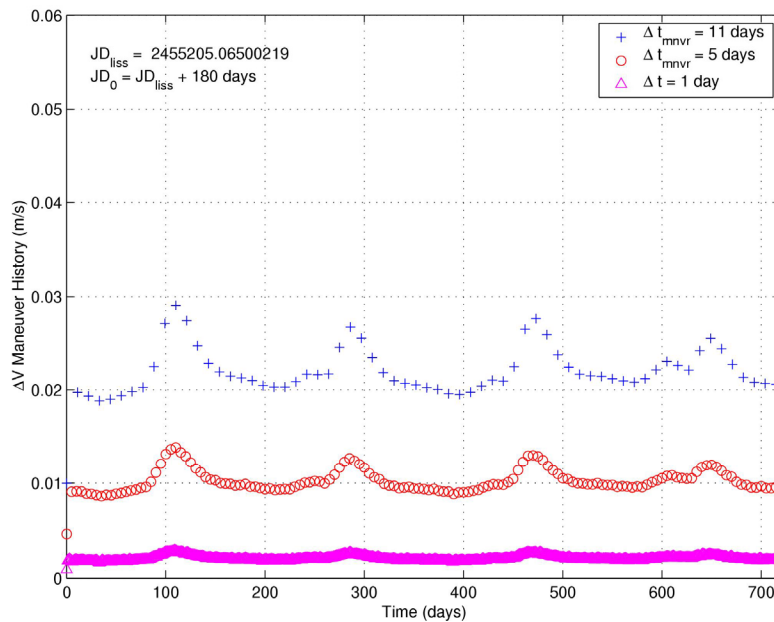for various maneuver intervals over two Earth cycles.**

**Figure 4 – Station keeping maneuver strategy
for a 100 km two s/c formation aligned with inertial *y*-axis.**

Note, from Figure 3, that during the wait period between maneuvers the trajectory diverges quickly from the pre-specified nominal path. Naturally, the maximum error incurred over each segment decreases as the scheduled time between maneuvers decreases. In spite of this trend, these results indicate that, if the nominal radial separation is large, continuous control is still required if a good level of accuracy is desired. Smaller formations, on the other hand, may benefit from a discrete approach.

For instance, consider a formation characterized by $\bar{\rho} = \left(10\ \text{m}\right)\hat{Y}$ and $\dot{\bar{\rho}} = \bar{0}$. As depicted in Figure 5, the maximum deviation achieved between maneuvers is significantly smaller, dropping below 10^{-2} m for maneuvers scheduled at least every 2 days. However, the magnitude of the individual maneuvers, illustrated in Figure 6, has decreased by several orders of magnitude, compared to the maneuvers in Figure 4. In practice, the error introduced in any attempt to physically implement such small maneuvers may offset the benefits. In addition, the tolerances that are achievable with any impulsive approach, for a fixed maneuver schedule, depend on the nominal separation between the vehicles.
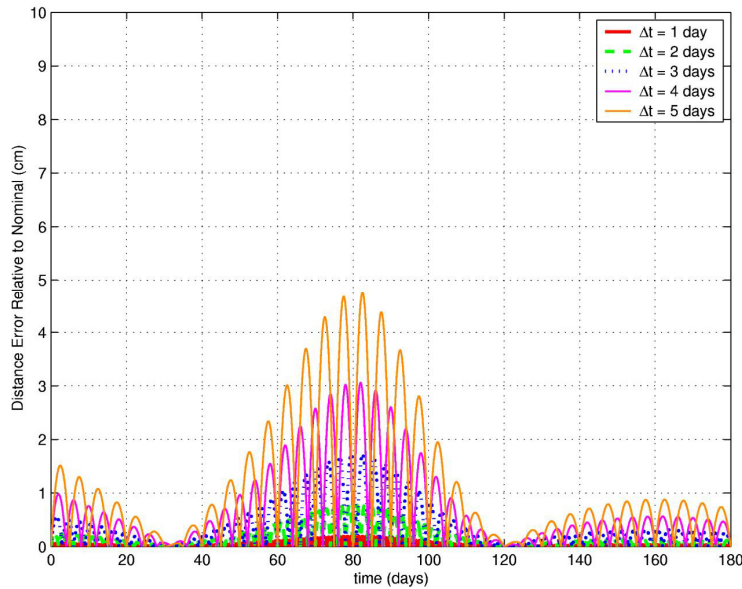
Figure 5 – Position error relative to the nominal path
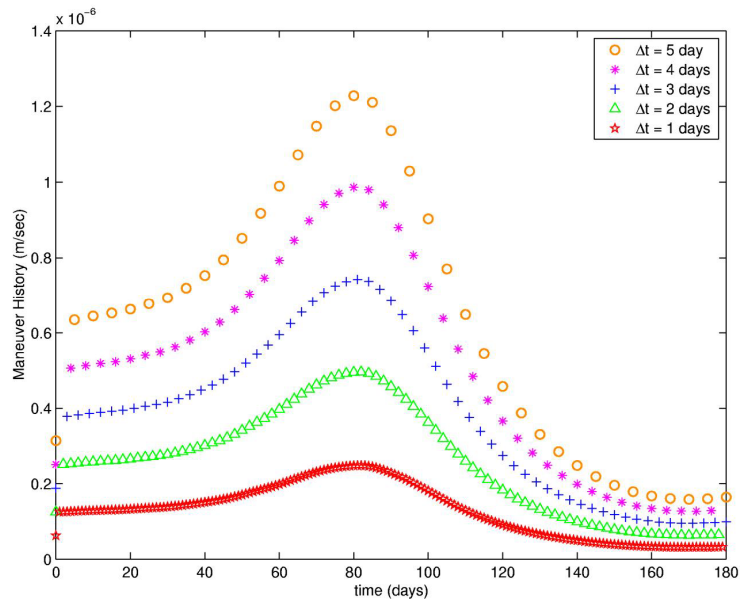**as a function of the length of the maneuver interval.**

Figure 6 – Station keeping maneuver strategy
(10 m two s/c formation aligned with inertial y-axis)

As observed from Figure 7, formation separations of up to 50 m can be achieved to within 10^{-2} m at all times, if a maneuver is performed once a day. If that interval is doubled to once every two days, then the maximum relative separation recommended drops to 15 m.
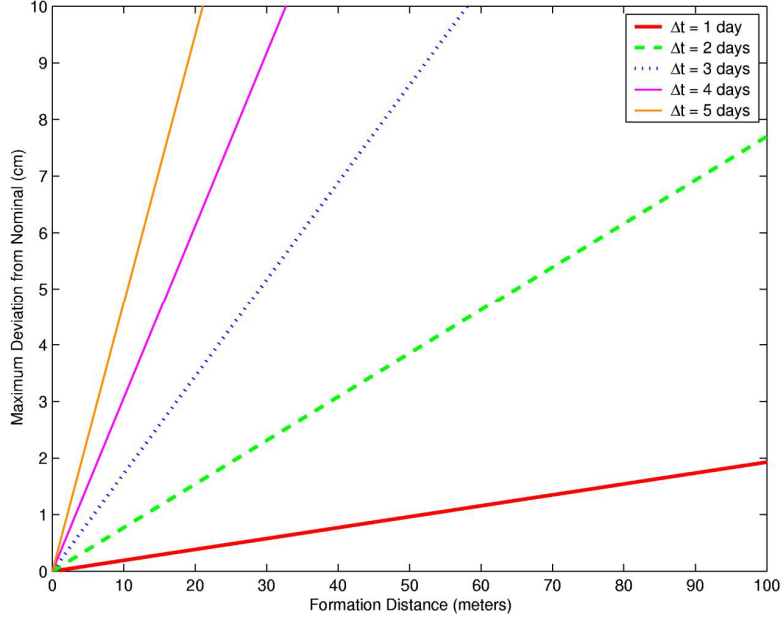

**Figure 7 – Maximum radial deviation
as a function of nominal formation distance and maneuver time interval.**

Targeting Radial Distance and Rate

Rather than the complete six-dimensional state vector, the number of targets is reduced and greater flexibility is introduced if functions of the states are constrained. Useful quantities here are the radial distance and/or radial rate between the deputy and chief vehicles. Let $\bar{x}_d(t)$ denote the six-dimensional state of the deputy spacecraft relative to the chief. This state may either be in inertial or rotating coordinates. Let the position elements of $\bar{x}_d(t)$ be denoted by $\bar{r}$ while the relative velocity is denoted as $\dot{\bar{r}}$. The radial distance and radial rates, then, are simply

$$r = \sqrt{\bar{r}^T \bar{r}} \,, \tag{1.6}$$

$$\dot{r} = \frac{\dot{\bar{r}}^T \bar{r}}{r} \,. \tag{1.7}$$

Let $\bar{g}^{\circ} = \left[r^{\circ}, \dot{r}^{\circ} \right]$ represent the desired range and range rate between the chief and deputy vehicles. Relative to this reference solution, a first order approximation of these quantities may be determined as

$$\bar{g} = \bar{g}^{\circ} + \frac{\partial \bar{g}}{\partial \bar{x}_d}(0) \delta \bar{x}_d(0) \,. \tag{1.8}$$

Equation (1.8) can be expressed as a function of the state transition matrix associated with the chief spacecraft,

$$\bar{g} - \bar{g}^{\circ} = \frac{\partial \bar{g}}{\partial \bar{x}_d}(t) \frac{\partial \bar{x}_d(t)}{\partial \bar{x}_d(0)} = \frac{\partial \bar{g}}{\partial \bar{x}_d}(t) \Phi(t, t_0) \,, \tag{1.9}$$

8

where

$$\frac{\partial \overline{g}}{\partial \overline{x}_d} = \begin{bmatrix} \dfrac{\partial r}{\partial \overline{r}} & \dfrac{\partial r}{\partial \dot{\overline{r}}} \\[2mm] \dfrac{\partial \dot{r}}{\partial \overline{r}} & \dfrac{\partial \dot{r}}{\partial \dot{\overline{r}}} \end{bmatrix}. \tag{1.10}$$

Let M define the state relationship matrix such that,

$$M = \frac{\partial \overline{g}}{\partial \overline{x}_d}(t)\Phi(t,t_0) = \begin{bmatrix} M_1 & M_2 \end{bmatrix} \tag{1.11}$$

where M_1 and M_2 are 2×3 matrices. Since the initial position, $\overline{r}(0) = \overline{r}_0$, is fixed, the associated variation, $\delta \overline{r}_0$, is zero. The velocity variation, then, can be determined from the minimum norm solution,

$$\delta \dot{\overline{r}}_0 = M_2^T \left(M_2 M_2^T \right)^{-1} \left(\overline{g}(t) - \overline{g}^{\circ}(t) \right) \tag{1.12}$$

Note that if the objective is control of only radial distance, then M_1 and M_2 are 1×3 matrices. Clearly, there are an infinite number of solutions that satisfy Equation (1.12). At any given time, solutions consistent with the constraints for radial distance and rate may or may not be contained within this solution space. The minimum norm approach seeks to identify the smallest maneuver that can achieve the desired goal at the end of each trajectory segment. To demonstrate the effectiveness of this targeter, consider the following example. Let the initial state of the deputy, relative to the chief spacecraft, be defined by $\overline{r}_0 = (5000 \text{ km})\hat{z}$ and $\dot{\overline{r}}_0 = \overline{0}$. Define the nominal range as 5000 km from the chief vehicle. Figure 8 includes three curves, each a time history for range, over 180 days, corresponding to one of three different correctors.
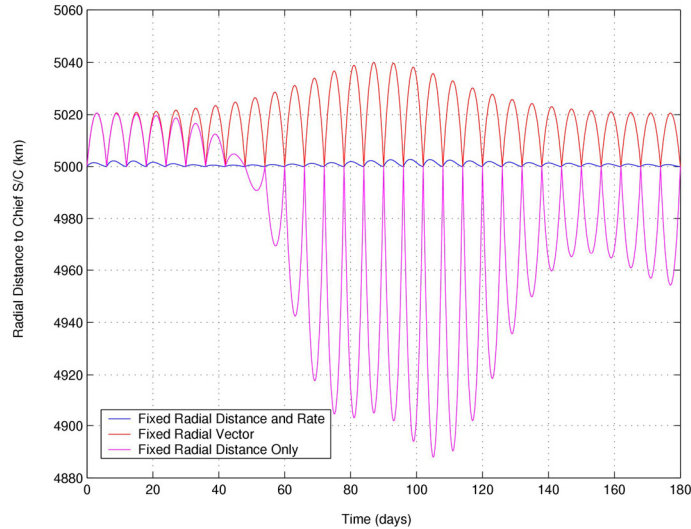

Figure 8 – Magnitude of Relative Position Error: Radial vs. State Targeter

The red curve is associated with the state corrector previously discussed. That is, the target state, at the end of each trajectory segment, is defined $\overline{r}^{\circ} = \overline{r}_0$ and $\dot{\overline{r}}^{\circ} = \overline{0}$. The blue trajectory, then, corresponds to the range error if only the radial distance and radial rate are constrained, for maneuvers determined from Equation (1.12). If, instead, the range rate is free, and only the radial distance is constrained, the magenta curve in Figure 8 demonstrates how the range error evolves over the duration of the mission.

9

Note that the differential corrector, in this third case, is essentially the same as that described by Equation (1.12) except the last row of M_2 is removed. Hence, the minimum norm solution is sought from one equation with three unknowns. The impulsive maneuver scheme associated with the results in Figure 8 appear in Figure 9. The size of the maneuvers and the total costs appear similar, but the excursions from the nominal are notably different, as observed from Figure 8. Since the overall error is significantly larger for the corrector that targets only range, the associated maneuver scheme is not included in Figure 9 and subsequent analysis.
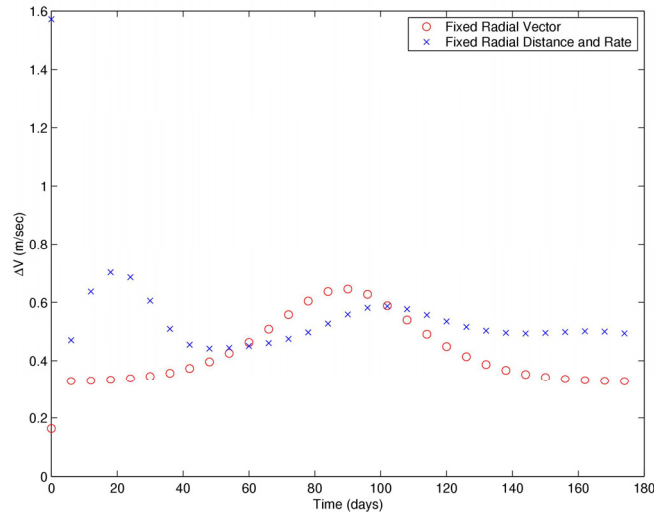
Figure 9 – Maneuver History: Radial vs. State Targeter

In any impulsive scheme, the path of the deputy <u>will</u> diverge from the desired nominal between maneuvers. An important observation, deduced from Figure 8, is that the degree of divergence depends on the nominal constraints imposed at the end of each trajectory segment. If minimizing the radial distance error over the length of each segment is desired, the range and range rate corrector offers a clear advantage over the other two correction schemes. Naturally, if maintaining the deputy at a constant distance and orientation, relative to the chief vehicle, is required to achieve the science goals of a particular mission, this type of corrections scheme is not adequate. This is best visualized in Figure 10.

The transparent blue sphere in Figure 10 represents the nominal radial distance constraint. The chief spacecraft is at the origin of this sphere. Now, nominally, at the end of each trajectory segment, the deputy is constrained to lie on this sphere and to approach this end point tangentially, $\dot{r} = 0$. Clearly, the natural dynamics allow for a radial distance that is very close to the nominal over the entire duration of the mission. However, in doing so, the deputy path is free to move anywhere along the nominal sphere.

The results and observations noted here are applicable regardless of the frame, inertial or rotating, in which the differential corrector is implemented, in either the CR3BP or EPHEM models. Of course, care must be exercised during the numerical implementation of any differential corrections process. In this case, inverting $\left(M_2 M_2^T\right)$ may lead to convergence difficulties in the corrections process, particularly over some trajectory segments, if the smaller singular value of M_2 approaches zero. So, it is best to delay the next maneuver until a more opportune time. Note that, as presently envisioned, a formation concept cannot benefit from this particular control approach if the nominal state for each deputy is completely specified. However, the results of this investigation are not exclusive to fixed state configurations or precision formation keeping.
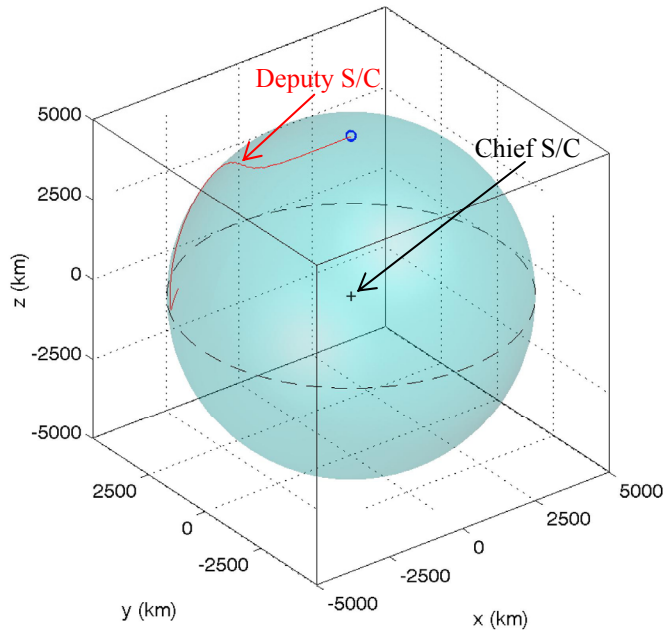
Figure 10 – Deputy S/C Path: Radial vs. State Targeter

In general, achieving the desired nominal configuration to extreme accuracy requires, at least, maneuvers that are fairly close to each other. As previously mentioned, as the maneuvers become more closely spaced they also decrease in size. So, regardless of whether continuous or discrete control is available, accurately maintaining a non-natural nominal configuration, with small relative separations, still requires very low thrust capabilities [34-37]. Delivering such small control inputs, accurately, may or may not be achievable with the technology presently available. Whether or not that is true depends on the required nominal path, any dynamical or mission specific constraints imposed on the formation, and the sensitivity of this analysis to modeling and measurement uncertainties as well as thrust implementation errors. Note, although allowing the solution to drift until a maneuver is sufficiently large to implement seems intuitive, this is not a feasible alternative in this regime. The highly sensitive natural flow in this region of space is constantly acting against these non-natural configurations.

Hence, regardless of how small the maneuvers may "appear", if they are not implemented accurately, the relative error quickly grows above the sub-millimeter range. This violates the tight formation keeping constraints presently envisioned for some of the proposed space-based interferometers. In contrast, formations that take advantage of the natural flow near the reference orbit require minimal station keeping beyond the initial injection maneuver.

FORMATIONS THAT EXPLOIT THE CENTER + STABLE MANIFOLDS

The center manifold that exists near the libration points allows for a variety of natural motions that could prove beneficial for formation flight. Lissajous trajectories and halo orbits are examples of motions that exist within the center manifold near L_1 and L_2. A Lissajous trajectory, for instance, allows for a phased natural formation whose geometry is analogous to a 'string of pearls'. To illustrate the concept, consider the Lissajous trajectory represented in Figure 11. The blue surface in Figure 11 is traced by a quasi-periodic Lissajous trajectory near the Sun-Earth/Moon L_2 point, as determined in the SRP perturbed n-body EPHEM model.

By properly phasing each vehicle, it is possible for the formation to naturally evolve along this surface such that the relative positions of each spacecraft in the formation are unaltered and the relative distances are closely bounded. That is, if the formation originates as a string of pearls, the orientation of the string is relatively unaffected in time, the lead vehicle always remains in the lead and the order of each subsequent vehicle along the 'string of pearls' remains unchanged.
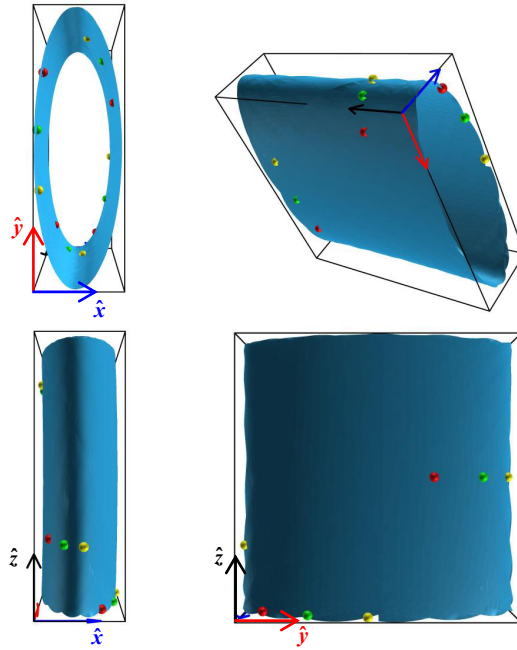
11

Figure 11 – Natural 'string of pearls' formation in the EPHEM model.

Since each spacecraft in this formation evolves along a naturally existing Lissajous trajectory, maintaining this type of formation can be achieved with a standard station keeping approach. Other relative motions can be numerically identified through a linear stability analysis of a reference solution near the libration points, such as a halo orbit in the CR3BP.

Howell and Marchand [31] develop two impulsive control schemes, based on Floquet analysis, that successfully deploy a vehicle into a variety of naturally existing formations. Either one of these controllers leads to motion that exhibits the overall features of the center subspace associated with the reference halo orbit (i.e., the nominal path of the chief spacecraft). The resulting trajectory arcs also exhibit features more commonly associated with motion along a stable manifold. As a direct result, the methodology employed by Howell and Marchand [31] not only defines potential nominal configurations, but also potential deployment into these configurations, as is demonstrated below.

In general, center modes are indicative of the existence of bounded solutions in the vicinity of the reference orbit. In the CR3BP, a periodic halo orbit is characterized by a four dimensional center subspace. Let $\bar{e}_j$, for $j = 4,\ldots,6$, denote a vector basis that spans the center subspace of the reference halo orbit. (Each eigenvector $\bar{e}_j$ contain six elements.) Modes $\bar{e}_5$ and $\bar{e}_6$ are associated with neighboring periodic halo orbits. Modes $\bar{e}_3(t)$ and $\bar{e}_4(t)$ span a two-dimensional subspace associated with solutions that evolve along a hollow two-dimensional (2-D) torus, known to envelop the halo orbit, as illustrated in configuration space in Figure 12.

This type of torus exists both in the CR3BP and in the EPHEM model and represents a natural (unforced) solution to the nonlinear equations of motion. In fact, the solution illustrated in Figure 12 is associated with the EPHEM model. If the initial relative state of the deputy is entirely contained within the subspace spanned by $\bar{e}_3$ and $\bar{e}_4$, then its path, relative to the halo orbit, is bounded and evolves along a torus, such as that illustrated in Figure 12. The deputy path presented in Figure 12 is measured relative to an observer fixed at the libration point. The relative path that defines the motion of the deputy, with respect to the chief, is best visualized from Figure 13. Relative to the chief spacecraft, Figure 13 depicts, as a surface, the trajectory along which the deputy evolves. In this depiction, the chief S/C is always located at the origin.
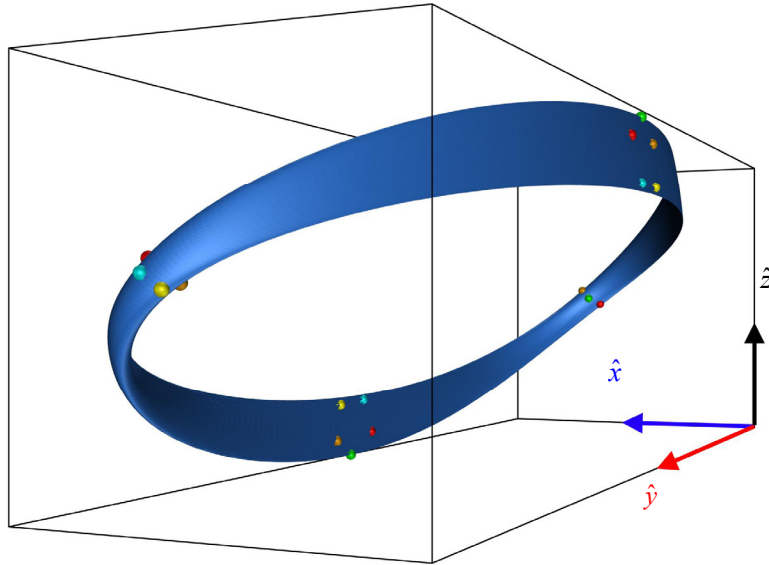
Figure 12 – Six spacecraft formation evolving along two-dimensional torus near L_1 in the Sun-Earth/Moon EPHEM model.
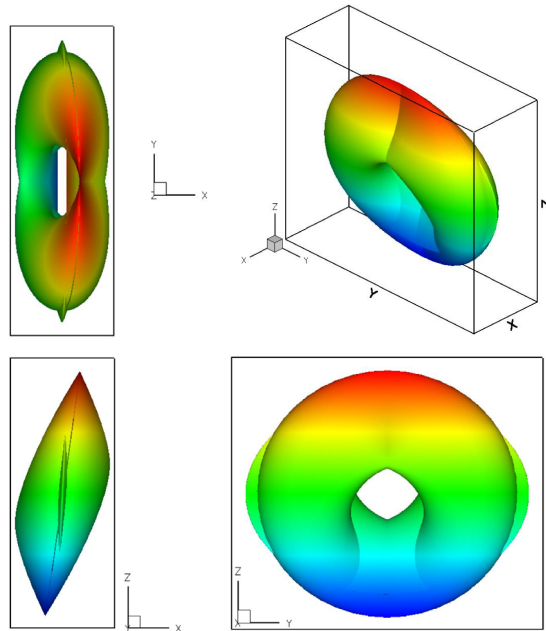

Figure 13 – Relative deputy motion along center manifold.

Note that the solution in Figure 13 is self-intersecting, but that is merely a product of the projection of the full six-dimensional states onto three-dimensional configuration space. Furthermore, although the solution illustrated in Figure 13 is generated in the linear system, it is known to represent a natural solution to the nonlinear equations both in the CR3BP and in the EPHEM model, as observed in Figure 12.

13

Application: Floquet controller to deploy into quasi-periodic torus formation

Consider a two-vehicle formation where the chief spacecraft is assumed to evolve along a 2×10^5 km halo orbit near the Sun-Earth/Moon L_1 point. Both spacecraft are deployed and arrive simultaneously at different points along the rotating xz-plane. Let the 'arrival' point for both spacecraft be defined as the point where they cross the xz-plane near the reference orbit. The position of the deputy spacecraft upon arrival is similar to the chief but 50 m off along the $+\hat{x}$ direction. The relative velocity of the deputy is not important, only the relative location of the two spacecraft is relevant. Once at the arrival point, the deputy spacecraft performs its first formation keeping maneuver [31]. This maneuver is the largest and is meant to place the spacecraft state into the desired subspaces. The magnitude of the maneuver is approximately equal to the magnitude of the relative velocity of the deputy with respect to the chief. For this particular example, the initial relative velocity of the deputy is selected as $\dot{\bar{r}}(0)=(\hat{x}-\hat{y}+\hat{z})$ ms^{-1}. Thus, the first maneuver of the deputy vehicle is $\left|\Delta\bar{V_1}\right|=1.73$ ms^{-1}. Thereafter, the trajectory of both the chief and deputy spacecraft requires a small deterministic $\Delta\bar{V}$ every 180 days (one orbital period along the halo orbit). For the chief spacecraft, these are necessary to enforce the periodicity condition over 100 orbital periods (and may simply be a numerical artifact). All of these corrections – both for the chief and deputy – are on the order of 10^{-8} ms^{-1}. The resulting path is illustrated in Figure 14. The first leg of the deputy path is most greatly influenced by the stable mode (2), while the converged path is consistent with the motion associated with modes five and six, previously illustrated in Figure 13.
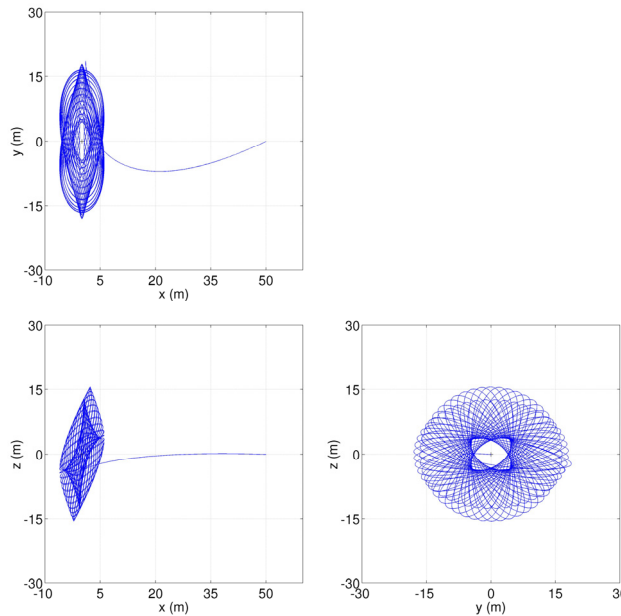

Figure 14 – Deployment into toroidal formation
(initial state excites only modes five and six).

Application: Floquet controller to deploy into nearly periodic formations

For the same reference halo orbit employed in the previous example, consider three deputies deployed along with the chief spacecraft. Each deputy spacecraft arrives simultaneously at a different location relative to the chief. In particular, the relative position vectors are 50 m, 100 m, and 140 m along the $+x$-direction. Application of the Floquet controller [31] leads to a nearly periodic formation. Once again, the first leg along the path of each deputy resembles motion along the stable manifold associated with the reference halo orbit.

However, the converged path is nearly periodic, as observed from Figure 15. The resulting path is propagated for ten revolutions of the reference halo orbit (1800 days). Beyond the initial injection maneuver, numerical corrections are implemented once every 180 days, although the magnitude is small (10^{-8} ms^{-1}).
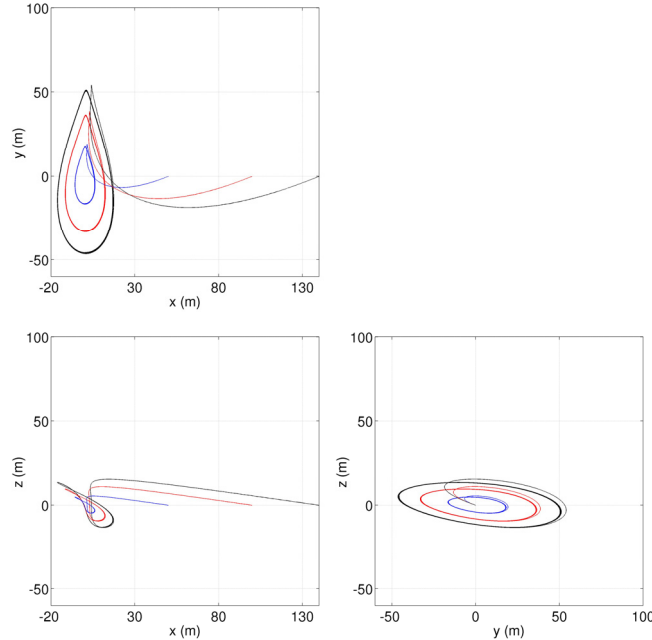

Figure 15 – Deployment into nearly periodic formation
(initial state excites only modes three and four).

The converged segment of the path in Figure 15 reveals a variety of nearly periodic solutions in the vicinity of the chief spacecraft. Since the controller forces these solutions to remain within a subspace spanned by $\overline{e}_2$, $\overline{e}_5$, and $\overline{e}_6$, the resulting path is not evolving solely along the halo family but rather along another type of nearly periodic motion in the vicinity of the reference halo orbit. This is most apparent as the amplitude of the relative orbits is increased above 10^3 km. To better visualize the potential configurations, Figure 16 illustrates eight deputies evolving along these nearly periodic orbits. Depending on the desired orbit amplitude, the actual path of each vehicle expands away from the chief spacecraft, but at a very slow rate. So, the individual orbits can be propagated for 100 revolutions of the reference halo, in the CR3BP, and will still appear periodic if the relative separations are small.

Let $\overline{r}(t)$ denote the relative position vector that locates the deputy with respect to the chief spacecraft. The orbits depicted in Figure 16 are obtained by applying the controller to a relative position vector of the form $\overline{r}(0) = r_0 \hat{y}$, where r_0 denotes some initial separation between the chief and deputy spacecraft. The rate of expansion of these relative orbits is more noticeable if the initial position vector originates anywhere else in the yz-plane. In fact, the rate of expansion reaches a maximum if the initial relative position vector is of the form $\overline{r}(0) = r_0 \hat{z}$. In this case, the resulting orbits appear nearly vertical and are illustrated in Figure 17 using a four spacecraft formation as an example. In the yz-projection, it is apparent that the expansion proceeds clockwise since, in this case, the reference orbit is a northern L$_1$ halo orbit. This is consistent with the direction of motion both along the halo family and the stable manifold in this region of space.
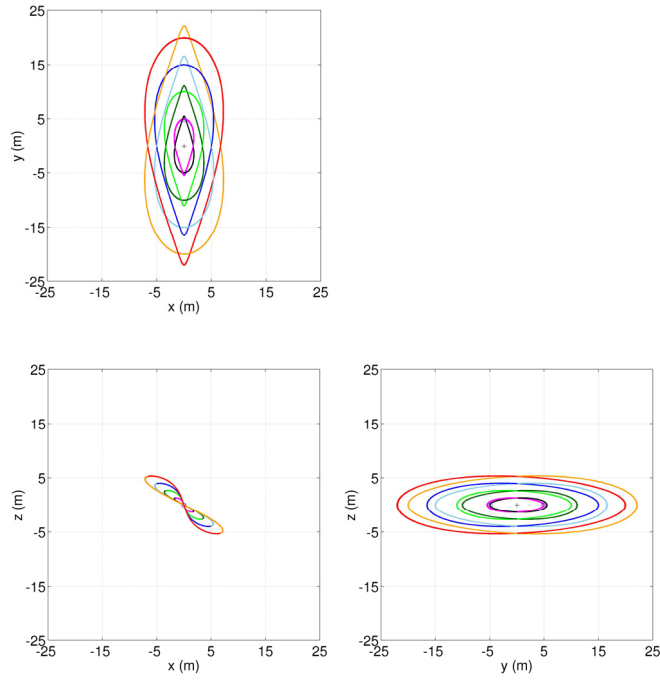
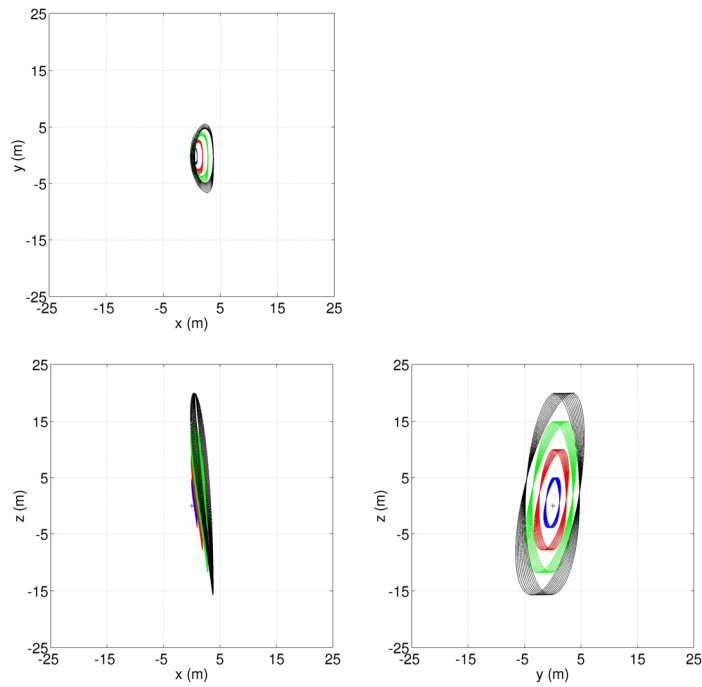**Figure 16 – Natural eight s/c formation about a single chief s/c.**

Figure 17 – Nearly vertical relative orbits (four S/C Formation).

Figure 18 further illustrates how the rate of expansion changes as the initial state is shifted throughout the *yz*-plane. The relative paths of the deputy, illustrated in Figure 18 (a), are determined in the CR3BP, based on the Floquet analysis [31] previously discussed. These trajectories serve as an initial guess to a two-level differential corrections process, developed by Howell and Pernicka [38], used to numerically identify the equivalent solutions in the EPHEM model. The solutions associated with the SRP perturbed EPHEM model are illustrated in Figure 18 (b). The sphere at the origin (the location of the chief) is included only to aid in visualizing the path of the deputy. Note that with no initial *z*-component, the orbit of the vehicle is periodic in the CR3BP and nearly periodic in the EPHEM model. As an out-of-plane component is introduced into the initial state, the resulting trajectory blends the characteristics of the orbits in both Figure 16 and Figure 17. Further propagating a nearly vertical orbit, characterized by $\bar{r}(0) = r_0 \hat{z}$, over a period of 100 revolutions (49.2 years) yields the surface illustrated in Figure 19.
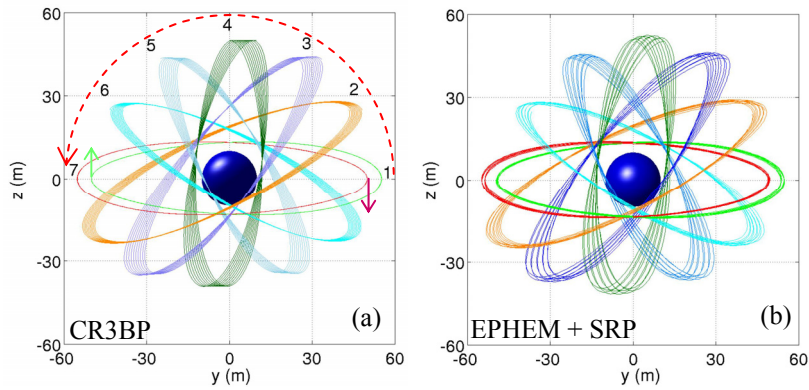

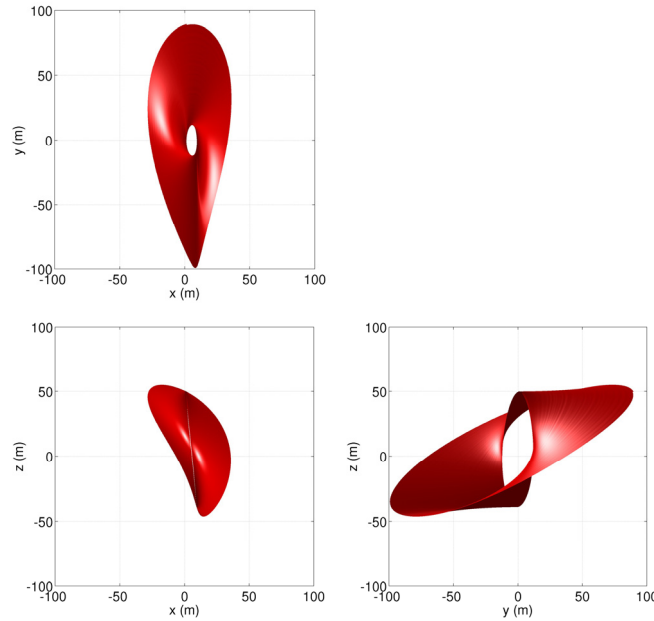**Figure 18 – Variation in relative orbit expansion rate along the yz-plane.**

Figure 19 – Evolution of nearly vertical orbit over 100 revolutions (49.2 years).

BLENDING NATURAL AND NON-NATURAL MOTIONS

Approach #1: Impulsive Formation Keeping

The naturally existing motions previously presented are employed here to simplify the process of identifying non-natural configurations. For instance, consider the sample relative deputy trajectories plotted in Figure 20 (a)-(c). These trajectories are determined in the EPHEM model both with and without SRP. As deduced from this figure, the relative path of the deputy is, clearly, not periodic. However, as an initial guess, it is sufficiently close to periodic if the effects of SRP are small. In this case, a differential corrector with end point constraints, developed by Wilson and Howell [39], is applied to enforce periodicity through a series impulsive maneuvers.
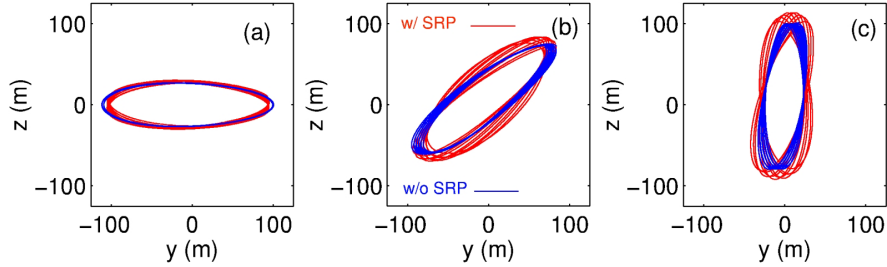

Figure 20 - Natural formations in the EPHEM model (w/ SRP).

Consider the first two revolutions (without SRP) in Figure 20 (b) and identify this trajectory segment as $\Gamma(T_1)$, where T_1 represents the approximate period. Let $\bar{x}_i(t_0) = \bar{x}(t_0)$ and $\bar{x}_e(t_m) = \bar{x}(t_m)$ denote the initial and final states along $\Gamma(T_1)$, respectively, and let $\bar{x}(t_k)$, for $k = 1,\ldots,m-1$, denote a discrete set of interior states such that $t_0 < t_k < t_m$. Since $\Gamma(T_1)$ is nearly periodic, replace the final state, at time t_m, with the initial state such that $\bar{x}_e(t_m) = \bar{x}_0(t_0)$. This set of $m+1$ patch states serves as an initial guess to the differential corrector developed by Wilson and Howell [39]. In the first level of this process, each trajectory segment is integrated from $t_k \to t_{k+1}$, for $k = 0,\ldots,m-1$. A simple differential corrections process seeks to achieve position continuity while allowing a maneuver at each patch state, $\Delta\bar{V}_k$. The next level of the corrector allows the position of each patch state to "float" seeking to reduce the interior maneuvers and meet the end point constraint.

Once the differential corrections process converges on a solution, the resulting patch states are shifted forward in time by T_1. This new set of patch states is then differentially corrected, as before, to enforce periodicity over the new time interval in the EPHEM model. The resulting trajectory is represented by $\Gamma(T_2)$. Since the initial and final states are always fixed, the individual trajectory arcs, $\Gamma(T_q)$, for $q = 1,\ldots,N$, can later be patched together for position continuity over N revolutions. The velocity discontinuities at the interior nodes, where $\Gamma(T_q)$ and $\Gamma(T_{q+1})$ intersect, represent impulsive maneuvers. Once the desired number of revolutions is achieved, the patch states along each arc can be merged into one set of patch points and differentially corrected simultaneously. This time, a maneuver is allowed at the connecting nodes between each $\Gamma(T_q)$. A sample solution, over six revolutions, is plotted in Figure 21 and is generated by applying two impulsive maneuvers ranging in size from 2.5 m/sec to 5 m/sec at the end of the second and fourth revolutions. Note that periodicity, in this case, is enforced in the Earth-centered rotating frame and one period encompasses two revolutions along the orbit.

A similar approach can be applied to the nearly vertical trajectory in Figure 20 (c) to obtain vertical periodic relative orbits; the result is plotted in Figure 22. This particular approach works very well if periodicity is enforced in the rotating frame as demonstrated in Figure 21 and Figure 22, as opposed to the inertial frame. Relative to an observer fixed in the rotating frame, these solutions appear to be sufficiently close to periodic and are, subsequently, a suitable initial guess for the differential corrector. However, the associated inertial perspectives that appear in Figure 23, are quite different. These trajectory arcs do not represent a sufficiently accurate initial guess if periodicity is required in the inertial frame. The natural geometry of the solution is such that the inertial and rotating views of the same trajectory are quite different. Of course, the Earth is at a different location in its orbit every time a revolution is completed, as opposed to a perspective originating in the rotating frame.
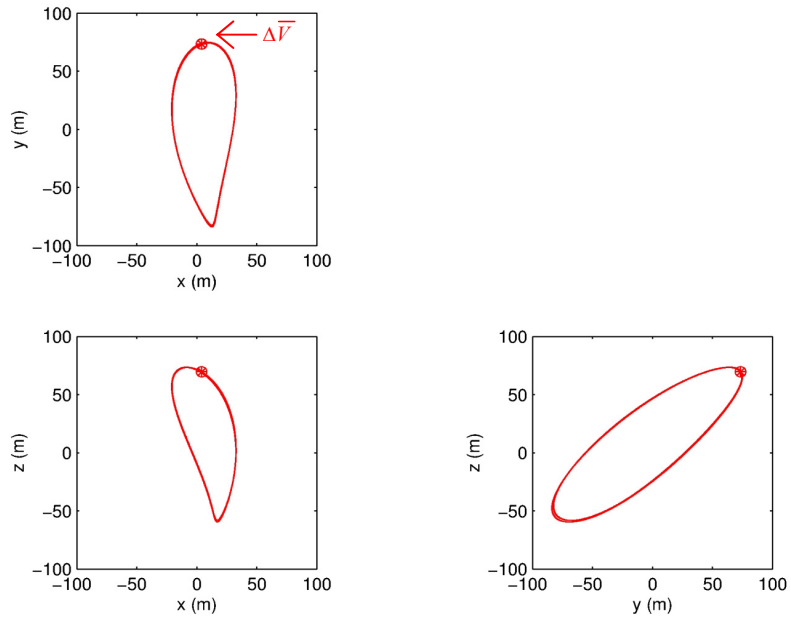
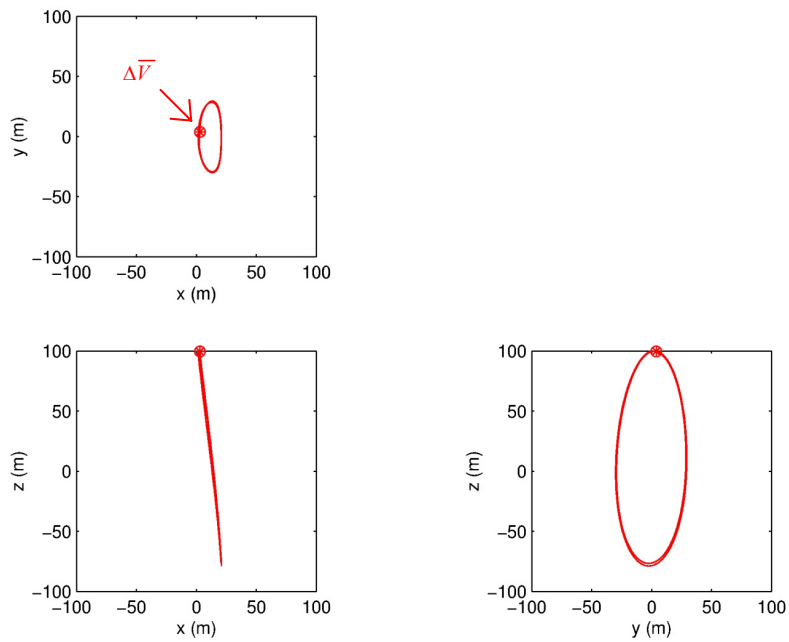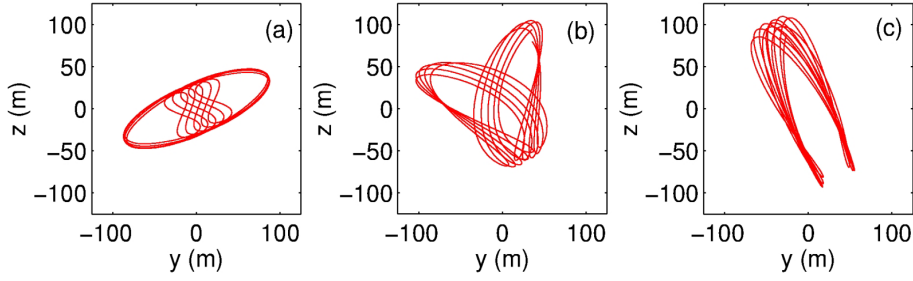**Figure 21 – Controlled periodic orbit in the EPHEM model (w/o SRP)**

Figure 22 – Controlled vertical orbit in the EPHEM model (w/o SRP).

Figure 23 – Natural formations in the EPHEM model (w/ SRP)
(inertial frame perspective of figures 11a-c).

Approach #2: Continuous Formation Keeping + Natural Trajectory Arcs

As previously noted, enforcing certain types of non-natural configurations may not always be possible via impulsive control alone. However, continuously operating the on-board thrusters may be inconvenient as well, depending on the constraints imposed on a particular mission. In these cases, a hybrid method may prove beneficial. That is, a method that employs continuous control as necessary, but takes advantage of the natural dynamics whenever possible. To illustrate this concept, consider feedback linearization as one possible continuous control methodology.

Feedback linearization, as discussed in Slotine and Li [40], is a nonlinear control strategy that allows the designer to pre-specify the desired response characteristics. This is accomplished, first, by applying an input that cancels the nonlinear terms in the equations of motion. A second term is subsequently added such that the desired response characteristics are satisfied.

Although canceling the nonlinear terms may, in general, lead to prohibitive control levels, the dynamical sensitivity characteristic of the region of space near the libration points creates an environment well suited to this particular approach. Of course, any form of feedback linearization requires full-state feedback, one of the disadvantages of the approach. However, for formation flight, if accurate relative state information is available, this method can be a powerful tool. Consider the equations of motion in Equation (1.1). It is possible to select $\bar{u}_d(t)$ such that the state follows a critically damped error response that meets some prescribed settling time requirement. For instance, let the response be characterized by a natural frequency ω_n. This frequency represents a design parameter and is selected to yield the desired settling time. The control law that achieves the desired response characteristics, and converges onto the prescribed nominal path, is determined as

$$\bar{u}_d(t) = \ddot{\bar{r}}^{\,\circ} - 2\omega_n\left(\dot{\bar{r}} - \dot{\bar{r}}^{\,\circ}\right) - \omega_n^{\,2}\left(\bar{r} - \bar{r}^{\,\circ}\right) - \Delta\bar{f}\ . \tag{1.13}$$

In this study, an acceptable response is one that reaches the desired solution within a day – assuming the position injection errors are not unreasonably large. A non-dimensional angular frequency (ω_n) of at least 1000 meets this requirement. It should be noted that decoupled control of each state variable is not necessarily the "optimal" solution, it is simply a way to accomplish the tracking goal. Howell and Marchand [30] demonstrate that, through this decoupling, the IFL control law in Equation (1.13) can yield almost identical results to the more traditional linear quadratic regulator (LQR) approach. However, Equation (1.13) offers a closed form solution for the control law that can be computed on demand during the numerical integration. An LQR approach requires, first, that the appropriate gain matrices (for the time varying linear system) be computed based on the nominal solution. The results of this process are then stored and accessed on demand during the actual numerical integration of the true deputy path. From a computational perspective, this particular characteristic makes IFL an appealing option.

In this study, natural motions are employed as an initial guess in identifying non-natural trajectory arcs that may be of interest for applications to formation flight. For instance, consider the solution labeled "4" in Figure 18. Clearly, this natural solution arc is not periodic. However, as previously described, it is possible to implement a differential corrections process to identify the impulsive maneuver scheme necessary to enforce a closed deputy path, as illustrated in Figure 22. Of course, the effectiveness of a differential corrections process is strongly dependent on the geometry of the local phase space and the existence of nearby solutions that satisfy the desired constraints. For instance, the natural solution arcs illustrated in Figure 23, as seen in the chief-centered ephemeris inertial frame, do not represent a good initial guess to a differential corrections process that seeks to enforce a closed or nearly periodic path via impulsive control. If impulsive control alone cannot accomplish the task, but continuous thruster operation does not represent a feasible option, a blending of methodologies may be sufficient to achieve the desired goals.

Consider, once again, the natural solution arc labeled "4" in Figure 18, but let $\bar{r}(0) = (500 \text{ m})\hat{z}$. Though the initial conditions are different, the shape of the solution is not affected, only the overall size of the orbit. The Floquet controller previously developed by Howell and Marchand [31] allows for the identification of the appropriate relative initial state associated with this nearly vertical path. Since the relative deputy path is not periodic, after one revolution (180 days) the path does not repeat. Suppose that continuous control is available over half a revolution (90 days). The goal, then, is to identify a continuous control law such that the path of interest is mirrored about some initial plane such that the combined trajectory (natural+controlled) is periodic. In the present example, the nearly vertical trajectory in Figure 18 is used as an initial guess to a simple differential corrector. The goal of the corrector is to identify, after half a revolution, the initial state required to achieve a perpendicular *xz*-plane crossing after roughly 90 days. This initial state leads to the trajectory segment highlighted in red in Figure 24.

In the absence of additional control inputs, this trajectory arc is neither closed nor periodic. In fact, the deputy spacecraft leaves the vicinity of the chief after the perpendicular crossing is achieved. In this case, the geometry of the phase space near the chief vehicle is not favorable for targeting a periodic orbit based on this particular initial state. However, it is still possible to achieve the desired reference motion if continuous control is applied. The IFL control law in Equation (1.13) is employed here to force the deputy spacecraft to track a path, after the plane crossing, that is a mirror image of the first segment. This second trajectory segment is highlighted in Figure 24 in blue.
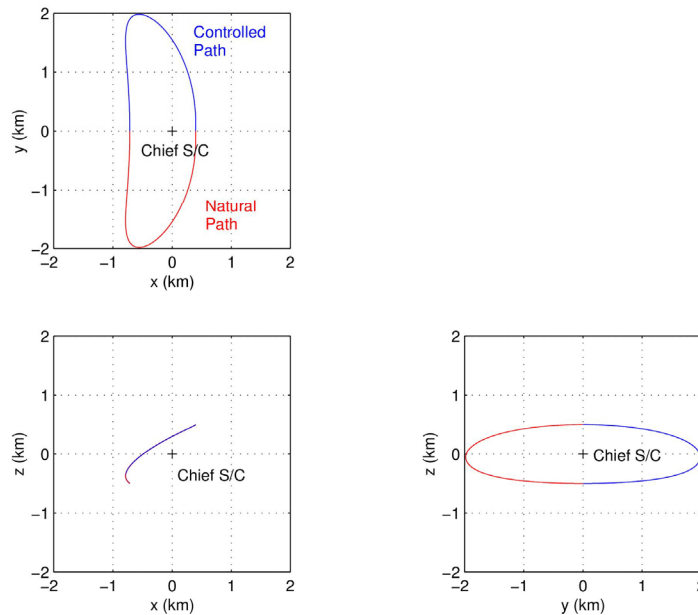

Figure 24 – Blending of Natural and Non-Natural Motions for Formation Applications

Implementation of this type of control requires that the reference motion be available as a function of time. Obviously, since no analytical solution exists in this regime, modeling the mirror path relies on numerical approximations. In this case, the mirrored time history of the state is stored and accessed based on cubic splines. The magnitude of the control acceleration required to enforce the solution in Figure 24 is illustrated in Figure 25.
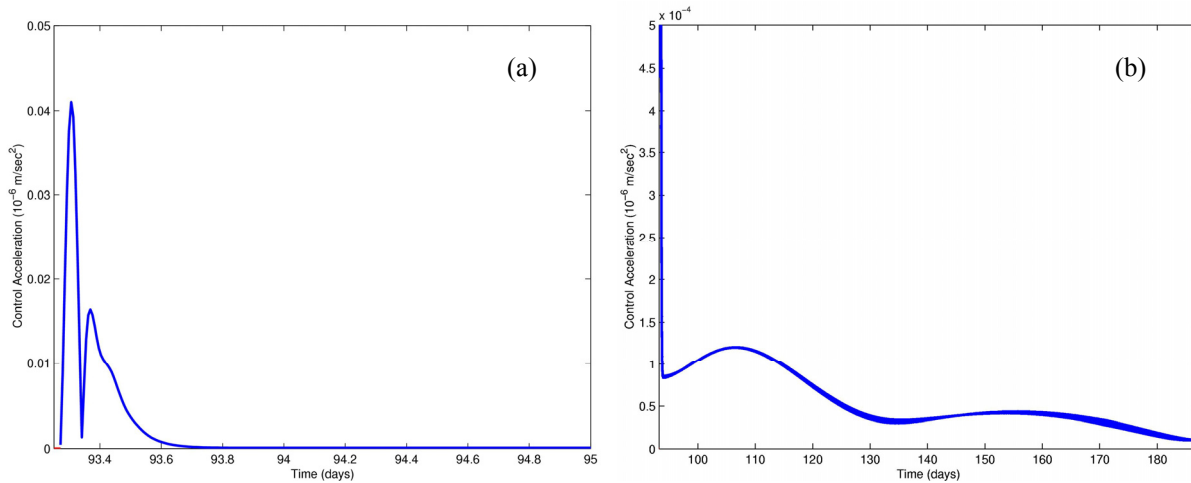

Figure 25 – Continuous Control Acceleration Profile
During Second Revolution along the Deputy S/C

The plot on the left hand side of Figure 25(a) shows the acceleration profile during the first few days after the plane crossing. The profile in Figure 25(b) is a close-up of the overall acceleration profile. The magnitude of the control accelerations is, in this particular example, very small. However, that is because the reference motion selected is not too far removed from the natural dynamics.

This example is presented only to illustrate how natural and non-natural arcs may be combined to achieve a non-natural solution using only partial continuous control over the duration of the path. Note that there is some error introduced in using splines to approximate the nominal path. However, as evidenced in Figure 25(b), the error is only noticeable when the control inputs are very small. This error is reduced by increasing the number of nodes used in the determination of the numerically approximated reference path.

CONCLUSIONS

Earlier stages of this study demonstrate the efficiency of continuous control methods as applied to non-natural formations in the n-body problem. Based on the available literature, it is clear that linear and nonlinear techniques, such as LQR and feedback linearization, can mathematically enforce a non-natural configuration in the n-body problem. However, continuous thruster operation does not always represent a desirable option. A difficulty inherent to the sensitive nature of this dynamical regime is that the accelerations levels required to maintain a non-natural configuration can be prohibitively small. Of course, whether or not this is true depends on the constraints imposed on the nominal formation dynamics. However small these control accelerations may seem, past studies suggest that accurate thrust delivery is crucial if precise formation keeping is sought. That is, if the relative position of the vehicles must be enforced at 10^{-2} meters or below. This dynamical sensitivity, though characteristic to this regime, can present many challenges for missions that require precise formation keeping but cannot rely on continuous thruster operation due to science constraints. In these cases, a hybrid control approach may be beneficial.

In this study, natural relative dynamics are combined with continuous control techniques to enforce non-natural motions without the need to apply continuous control over the duration of the mission. This allows for some thruster down times during which the science collection may proceed. Although this approach may, in theory, resolve some of the issues associated with precision formation keeping, it does not resolve all of them. For instance, the thrust levels may still be prohibitively small, depending on the desired reference path. In these cases, even with improved technology, the implementation error may be on the same order of magnitude as the thrust level, a potentially significant problem given the sensitivity of the dynamical response to small perturbations.

Precise formations, in fact, may not even be required, given a possible shift to improved navigation and relative position information. Hence, it is useful to explore the effectiveness of discrete control. For non-natural formations, a targeter approach is implemented here to maintain the desired configuration within a reasonable degree of accuracy. Not surprisingly, tightly spaced maneuvers are required to closely maintain a desired non-natural configuration. The frequency of the maneuver interval depends on the desired nominal separation between each spacecraft and any additional dynamical constraints imposed on the formation. Furthermore, achieving the desired accuracy, and the physical requirements to do so, present yet another dilemma. As previously stated, if maintaining a tight non-natural formation is desired, frequent maneuvers are necessary. However, smaller maneuver intervals require smaller maneuvers. The magnitude of these maneuvers, individually, is still extremely small.

The difficulties encountered with non-natural configurations may be overcome by developing a better understanding of the naturally existing formations. Of course, a nominal configuration that is <u>completely</u> consistent with the natural flow near the reference orbit may not satisfy all the dynamical requirements imposed by a particular mission. However, understanding these naturally existing behaviors can lead to the development of techniques to aid the construction of nominal formations that do meet the proposed mission objectives, while exploiting the natural structure. To that end, a modified Floquet based controller is successfully applied here that reveals some interesting natural formations as well as deployment into these configurations.

ACKNOWLEDGEMENTS

REFERENCES

[1] Vassar, R. H., and Sherwood, R. B., 1985, Formationkeeping for a pair of satellites in a circular orbit. *Journal of Guidance, Control, and Dynamics*, **8**, 235-242.

[2] Ulybyshev, Y., 1998, Long-term formation keeping of satellite constellation using linear quadratic controller. *Journal of Guidance, Control, and Dynamics*, **21**(1), 109-115.

[3] Chao, C. C., Pollard, J. E., and Janson, S. W., 1999, Dynamics and control of cluster orbits for distributed space missions. AAS/AIAA Space Flight Mechanics Meeting, 7-10 February 1999 (Breckenridge, Colorado: AAS). AAS Paper 99-126.

[4] Tan, Z., Bainum, P. M., and Strong, A., 2000, The implementation of maintaining constant distance between satellites in elliptic orbits. AAS/AIAA Space Flight Mechanics Meeting, 23-26 January 2000 (Clearwater, Florida: AAS), pp. 667-683.

[5] de Queiroz, M. S., Kapila, V., and Yan, Q., 2000, Adaptive nonlinear control of multiple s/c formation flying. *Journal of Guidance, Control, and Dynamics*, **23**(3), 385-390.

[6] Kapila, V., Sparks, A. G., Buffington, J. M., and Yan, Q., 2000, Spacecraft formation flying: dynamics and control. *Journal of Guidance, Control, and Dynamics*, **23**(3), 561-563.

[7] Yan, Q., Yang, G., Kapila, V., and de Queiroz, M. S., 2000, Nonlinear dynamics and output feedback control of multiple spacecraft in elliptic orbits. American Control Conference, 28-30 June 2000 (Chicago, Illinois: ACC).

[8] Wang, Z., Khorrami, F., and Grossman W., 2000, Robust adaptive control of satellite formationkeeping for a pair of satellites. American Control Conference, 28-30 June 2000 (Chicago, Illinois: ACC).

[9] Sparks, A., 2000, Satellite Formationkeeping Control in the Presence of Gravity Perturbations. American Control Conference, 28-30 June 2000 (Chicago, Illinois: ACC).

[10] Yedevalli, R. K., and Sparks, A. G., 2000, Satellite formation flying control design based on hybrid control system stability analysis. American Control Conference, 28-30 June 2000 (Chicago, Illinois: ACC).

[11] Stansbery, D. T., and Cloutier, J. R., 2000, Nonlinear control of satellite formation flight. AIAA Guidance, Navigation, and Control Conference and Exhibit, 14-17 August 2000 (Denver, Colorado: AIAA). AIAA Paper 2000-4436.

[12] Sabol, C., Burns, R., and McLaughlin, C., 2001, Satellite formation flying design and evolution. *Journal of Spacecraft and Rockets*, **38**(2), 270-278.

[13] Schaub, H., and Alfriend, K. T., 2001, Impulsive Spacecraft Formation Flying Control to Establish Specific Mean Orbit Elements. *Journal of Guidance, Control, and Dynamics*, **24**(4), 739-745.

[14] Irvin Jr., D. J., and Jacques, D. R., 2001, Linear vs. nonlinear control techniques for the reconfiguration of satellite formations. AIAA Guidance, Navigation, and Control Conference and Exhibit, 6-9 August 2001 (Montreal, Canada: AIAA). AIAA Paper 2001-4089.

[15] Vadali, S. R., Vaddi, S. S., Naik, K., and Alfriend, K. T., 2001, Control of satellite formations. AIAA Guidance, Navigation, and Control Conference and Exhibit, 6-9 August 2001 (Montreal, Canada: AIAA). AIAA Paper 2001-4028.

[16] Starin, S. R., Yedavalli, R. K., and Sparks, A. G., 2001, Spacecraft formation flying maneuvers using linear quadratic regulation with no radial axis inputs. AIAA Guidance, Navigation, and Control Conference and Exhibit, 6-9 August 2001 (Montreal, Canada: AIAA). AIAA Paper 2001-4029.

[17] Scheeres, D. J., and Vinh, N. X., 2000, Dynamics and control of relative motion in an unstable orbit. AIAA/AAS Astrodynamics Specialist Conference, 14-17 August 2000 (Denver, Colorado: AIAA). AIAA Paper 2000-4135.

[18] Gurfil, P., and Kasdin, N. J., 2001, Dynamics and control of spacecraft formation flying in three-body trajectories, AIAA Guidance, Navigation, and Control Conference and Exhibit, 6-9 August 2001 (Montreal, Canada: AIAA). AIAA Paper 2001-4026.

[19] Gurfil, P., Idan, M., and Kasdin, N. J., 2002, Adaptive neural control of deep-space formation flying. American Control Conference, 8-10 May 2002 (Anchorage, Alaska: ACC), pp. 2842-2847.

[20] Luquette, R. J., and Sanner, R. M., 2001, A non-linear approach to spacecraft formation control in the vicinity of a collinear libration point. AAS/AIAA Astrodynamics Conference, 30 July-2 Aug. 2001 (Quebec, Canada: AAS). AAS Paper 01-330.

[21] Hamilton, N. H., 2001, Formation flying satellite control around the L_2 Sun-Earth libration point. M.S. Thesis, George Washington University, Washington, DC, December 2001.

[22] Folta, D., Carpenter, J. R., and Wagner, C., 2000, Formation flying with decentralized control in libration point orbits. International Symposium: Spaceflight Dynamics, June 2000 (Biarritz, France).

[23] Barden, B. T., and Howell, K. C., 1998, Fundamental motions near collinear libration points and their transitions. *The Journal of the Astronautical Sciences*, **46**(4), 361-378.

[24] Barden, B. T., and Howell, K. C., 1998, Formation flying in the vicinity of libration point orbits. *Advances in Astronautical Sciences*, **99**(2), 969-988.

[25] Barden, B. T., and Howell, K. C., 1999, Dynamical issues associated with relative configurations of multiple spacecraft near the Sun-Earth/Moon L_1 point. AAS/AIAA Astrodynamics Specialists Conference, 16-19 August 1999 (Girdwood, Alaska: AAS), AAS Paper 99-450.

[26] Howell, K. C., and Barden, B. T., 1999, Trajectory design and stationkeeping for multiple spacecraft in formation near the Sun-Earth L_1 point. IAF 50th International Astronautical Congress, 4-8 October 1999 (Amsterdam, Netherlands: IAF/IAA). IAF/IAA Paper 99-A707.

[27] Gómez, G., Lo, M., Masdemont, J., and Museth, K., 2001, Simulation of formation flight near Lagrange points for the TPF mission. AAS/AIAA Astrodynamics Conference, 30 July - August 2 2001 (Quebec, Canada: AAS). AAS Paper 01-305.

[28] Howell, K. C., and Keeter, T., 1995, Station-keeping strategies for libration point orbits - target point and Floquet mode approaches. *Advances in the Astronautical Sciences,* **89**(2), 1377-1396.

[29] Gómez, G., Howell, K. C., Masdemont, J., and Simó, C., 1998, Station-keeping strategies for translunar libration point orbits. *Advances in Astronautical Sciences*, **99**(2), 949-967.

[30] Howell, K. C., and Marchand, B. G., 2003, Control strategies for formation flight in the vicinity of the libration points. AAS/AIAA Space Flight Mechanics Conference, 9-13 February 2003 (Ponce, Puerto Rico: AAS), AAS Paper 03-113.

[31] Marchand, B. G., and Howell, K. C., 2003, Formation flight near L_1 and L_2 in the Sun-Earth/Moon ephemeris system including solar radiation pressure. AAS/AIAA Astrodynamics Specialists Conference, 3-8 August 2003 (Big Sky, Montana: AAS). AAS Paper 03-596.

[32] Marchand, B. G., and Howell, K. C., 2004, Aspherical formations near the libration points of the Sun-Earth/Moon system. AAS/AIAA Space Flight Mechanics Meeting. 7-12 February 2004 (Maui, Hawaii: AAS). AAS Paper 04-157.

[33] McInnes, C. R., 1999, *Solar Sailing: Technology, Dynamics and Mission Applications* (United Kingdom: Praxis Publishing Ltd).

[34] http://space-power.grc.nasa.gov/ppo/projects/eo1/eo1-ppt.html.

[35] Mueller, J., 1997, Thruster options for microspacecraft: a review and evaluation of existing hardware and emerging technologies. 33rd AIAA/ASME/SAE/ASEE Joint Propulsion Conference & Exhibit, 6-9 July 1997 (Seattle, Washington: AIAA). AIAA Paper 97-3058.

[36] Gonzales, A. D., and Baker, R. P., 2001, Microchip laser propulsion for small satellites. 37th AIAA/ ASME/ SAE/ ASEE Joint Propulsion Conference and Exhibit, 8-11 July 2001 (Salt Lake City, Utah: AIAA). AIAA Paper 2001-3789.

[37] Phipps, C., and Luke, J., 2002, Diode laser-driven microthrusters - a new departure for micropropulsion. *AIAA Journal*, **40**(2), 310-318.

[38] Howell, K. C., and Pernicka, H. J., 1988, Numerical determination of Lissajous trajectories in the restricted three-body problem. *Celestial Mechanics*, **41**, 107-124.

[39] Wilson, R. S., and Howell, K. C., 1991, Trajectory Design in the Sun-Earth/Moon System Using Multiple Lunar Gravity Assists. *Journal of Spacecraft and Rockets*, **35**(2), 191-198.

[40] Slotine, J. E., and Li, W., 1991, *Applied Nonlinear Control* (New Jersey: Prentice Hall).